Shock Waves
https://doi.org/10.1007/s00193-018-0832-2

ORIGINAL ARTICLE

Shock wave and flame front induced detonation in a rapid compression machine

Y. Wang[1] · Y. Qi[1] · S. Xiang[1] · R. Mével[2,3] · Z. Wang[1,2,3]

Received: 1 November 2017 / Revised: 30 April 2018 / Accepted: 8 May 2018

Abstract
The present study focuses on one mode of detonation initiation observed in a rapid compression machine (RCM). This mode is referred to as shock wave and flame front-induced detonation (SWFID). Experimental high-speed imaging and two-dimensional numerical simulations with skeletal chemistry are combined to unravel the dominant steps of detonation initiation under SWFID conditions. It is shown that the interaction between the shock wave generated by the end-gas auto-ignition and the spherical flame creates a region of high pressure and temperature which enables the acceleration of the flame front and the detonation onset. The experimental observation lacks adequate spatial and temporal resolution despite good reproducibility of the detonation onset. Based on the numerical results, phenomenological interpretation of the event within the framework of shock wave refraction indicates that the formation of a free-precursor shock wave at the transition between regular and irregular refraction may be responsible for detonation onset. The present results along with previous findings on shock wave reflection-induced detonation in the RCM indicate that super-knock occurs after the interaction of the shock wave generated by end-gas auto-ignition with the RCM walls, preignition flame, or another shock wave.

Keywords Shock–flame interaction · Detonation · Rapid compression machine · Shock refraction

1 Introduction

Over the past 150 years, the continuous and increasing utilization of fossil fuel combustion for energy production has resulted in a significant reduction of reserves and a dramatic increase of greenhouse gas concentration and air pollution [1–3]. Limiting the impact of combustion processes to Earth's climate and air quality demands a significant improvement of the efficiency of combustion-based energy systems.

One strategy to improve the efficiency of the spark ignition internal combustion engine (SI-ICE) is to increase the power density through high boosting [4–6]. However, under such conditions, super-knock can occur and constitutes the major obstacle for the development of the next generation of SI-ICE [4]. Although it has been demonstrated by use of a rapid compression machine (RCM) that a detonation can be initiated during this process [4,5], the initiation mechanism remains unclear.

Combustion process in RCMs, and more generally in ICEs, is influenced by the inhomogeneity of the test volume induced by heat transfer and mixing [7–10]. Numerous studies have investigated the impact of reactivity gradient on the mode of propagation of combustion waves. In his pioneering analysis, Zeldovich [11] distinguished four modes of reaction: (1) weak detonation, (2) normal detonation, (3) subsonic flame not affected by heat conductivity, (4) normal flame. Bradley et al. [12] and Gu et al. [13] derived a detonation peninsula in the (ϵ, ξ) space from one-dimensional simulations performed under conditions representative of internal combustion engines at high load,

Communicated by G. Ciccarelli.

Electronic supplementary material The online version of this article (https://doi.org/10.1007/s00193-018-0832-2) contains supplementary material, which is available to authorized users.

✉ Y. Qi
qiyl@tsinghua.edu.cn

[1] State Key Laboratory of Automotive Safety and Energy, Tsinghua University, Beijing, China

[2] Center for Combustion Energy, Tsinghua University, Beijing, China

[3] Department of Automotive Engineering, Tsinghua University, Beijing, China

Published online: 22 May 2018

where ϵ is the ratio of acoustic time to the excitation time of local homogeneous mixture and ξ is the actual temperature gradient at the hot spot normalized by the critical gradient. More recently, Dai and Chen [14] and Dai et al. [15] studied reaction front propagation in n-heptane/air mixtures with a hot or cool spot using one-dimensional numerical simulations with a skeletal kinetic model containing low-temperature chemistry. They showed that both configurations could result in the initiation of a detonation wave. All of these previous studies employed theoretical approaches or one-dimensional numerical simulations and, despite providing important insight into the dynamics of end-gas auto-ignition and subsequent combustion wave propagation, they constitute an over-simplified description of the actual configuration in an ICE.

Although super-knock observation is simplified by using RCMs rather than optical engines, the initiation process remains highly three-dimensional and the details of the detonation onset are difficult to capture. In many cases, the super-knock event can be described as a succession of three steps. The first step corresponds to preignition [6]. Such an event may originate from the combustion of lubricating oil droplets ejected from the cylinder liner or from the oxidation/ignition of solid particles [6]. To increase the frequency of super-knock occurrence in an RCM, and facilitate its investigation, some studies have employed an electrical spark plug to mimic preignition [16]. The following step in the super-knock development process has been observed to be a near-wall auto-ignition within the end-gas [4,6,16]. The shock wave created by this localized explosion might then interact with the RCM walls, the expanding flame, or another shock wave formed by another quasi-simultaneous near-wall explosion. This interaction is the third step of the super-knock event and leads to the actual detonation onset. Depending on the kind of interaction that is taking place, different modes of detonation initiation may be distinguished. In a previous study [16], the dynamics of one mode of initiation, namely shock wave reflection-induced detonation (SWRID), has been revealed through high-speed direct photography in an RCM. This mode of initiation is characterized by the formation of a Mach reflection as the shock wave formed by a local end-gas explosion that propagates along the RCM wall. The high temperature and pressure behind the Mach stem trigger a detonation that propagates within the compressed end-gas and generates pressure oscillations.

The present paper focuses on another mode, referred to as shock wave and flame front-induced detonation (SWFID). We aim at clarifying the mechanism of this mode of detonation initiation which results from the interaction of the shock wave originating from end-gas auto-ignition with the flame expanding from the spark plug. Experimental work in an RCM and two-dimensional numerical simulations with skeletal chemistry are combined to unravel the dominant steps of the SWFID process.

2 Experimental and computational methods

2.1 Rapid compression machine

Super-knock experiments were conducted in an RCM at Tsinghua University. A detailed description of the experimental setup and the data processing procedure can be found in Di et al. [17]. Briefly, the RCM has a fixed stroke of 500 mm and a combustion chamber diameter of 50.8 mm. The mixture in the test section was brought to high pressure and temperature within 30 ms, with the last half of the pressure rise in less than 4 ms. A creviced piston design was used to minimize the effect of the roll-up vortex. A piezoelectric pressure transducer (Kistler 6125C) and quartz window were mounted on the side and end wall of the combustion chamber, respectively. The images were recorded using a high-speed camera (Photron SA-X2) at a framing rate of 288 kfps (frame interval of 3.47 μs). The spark plug (Denso K20R) was mounted opposite to the pressure sensor with electrodes located at the center of the combustion chamber to generate a flame and was triggered at the end of compression (EOC). The schematic of the RCM is shown in Fig. 1.

2.2 Test mixture

For all experiments, a stoichiometric iso-octane/air mixture was used, i.e., the molar ratio of iso-C_8H_{18}:O_2:N_2 was 1:12.5:47. High-purity nitrogen (> 99.999%), oxygen (> 99.995%), and iso-octane (> 99%) were employed. The mixture was prepared in a dedicated stainless steel mixing tank at room temperature using the partial pressure method. The liquid fuel was injected into the mixing tank through a PTFE septum. Before a series of experiments, the mixture was left to homogenize by diffusion for 12 h. The compression ratio in this study was fixed at 9.8. Thus pressure at the EOC was varied by changing the initial pressure while the temperature was kept consistent. A typical condition in which SWFID occurred was 641 K and 2.5 MPa at the EOC, which was also used in the numerical study.

2.3 Numerical simulations

2.3.1 Reaction model

The chemical kinetics model employed was a skeletal primary reference fuel (PRF) model, referred to as generalized research octane number (GRON) model [18]. It is composed of 22 species and 21 reactions. Details about the construction of the GRON model were given in Wang et al. [18].

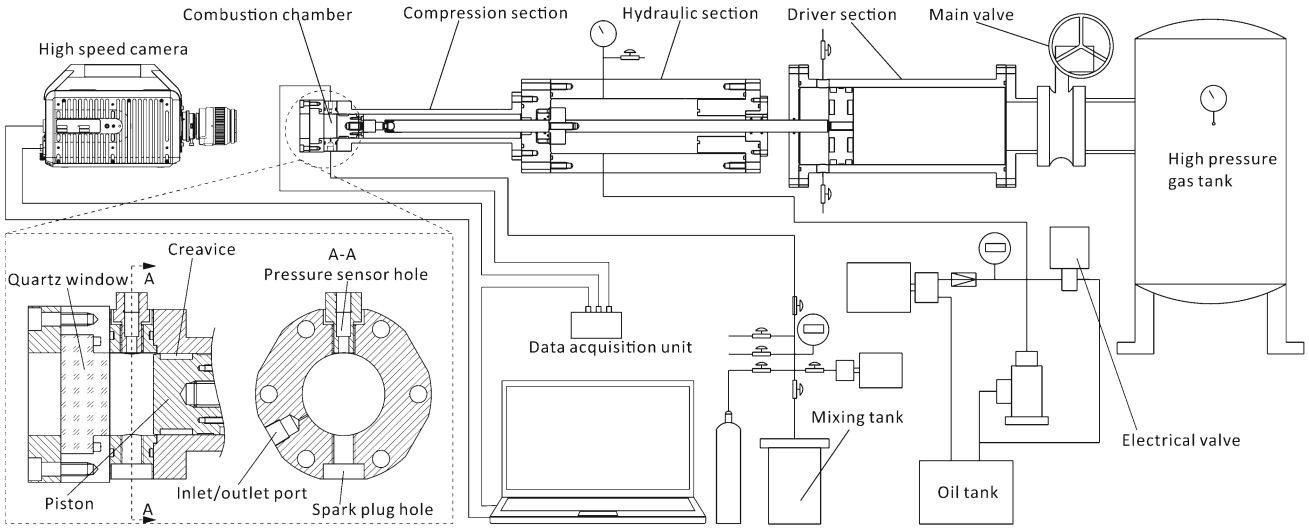

Fig. 1 Schematic configuration of the rapid compression machine [5]

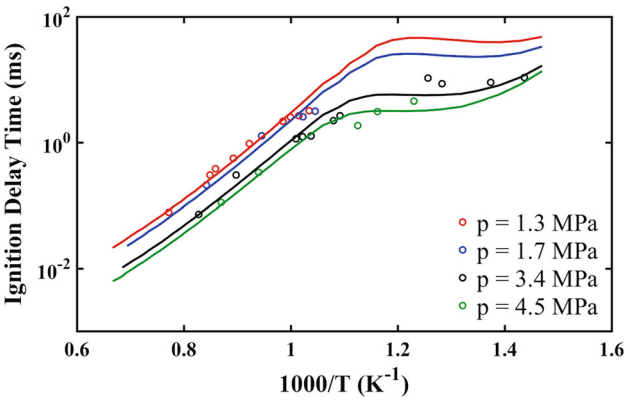

Fig. 2 Validation of the GRON model for iso-octane–air mixtures. Experiments taken from [21]

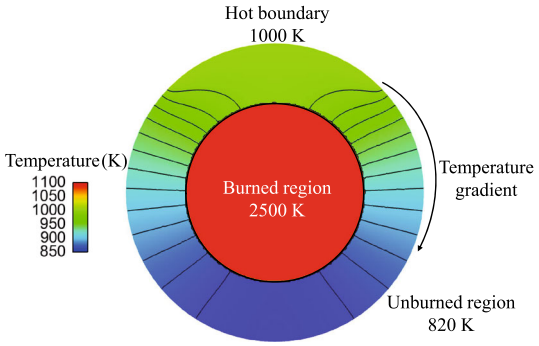

Fig. 3 Schematic of the computational domain with initial and boundary conditions. The solid lines represent iso-contours of temperature

Briefly, the GRON model builds on the skeletal models from Tanaka et al. [19] and Tsurushima [20]. Taking advantage of the similar behavior of PRFs in the high-temperature range, the GRON model includes a common base of 19 reactions to describe the auto-ignition process above 1000 K. The ignition behavior specific to a RON number in the intermediate- and low-temperature range is controlled by adjusting the rates of the initiation reaction: $RH + O_2 = R + HO_2$ and QOOH radical formation: $R + O_2 = QOOH$. Figure 2 compares the experimental and calculated ignition delay time of stoichiometric iso-octane/air mixture at different pressures. Quantitative agreement is observed with a mean absolute error on the order of 21%.

2.3.2 Computational methods

The CONVERGE code with adaptive mesh refinement (AMR) method [22] was used to simulate this process. Considering the compromise of detonation length scale and computational cost, a self-adaptive mesh with a basic grid size of 0.2 mm and a minimum of 25 μm was used. Adiabatic nonslip boundary conditions were applied at the wall, while the initial conditions were derived from the experiments. The measured pressure at the onset of auto-ignition was 7.46 MPa. Assuming an isentropic compression of the fresh mixture during the propagation of the spherical flame, the temperature was calculated to be 820 K in the unburnt end-gas region. In the burnt region, a complete combustion assumption was employed with the temperature of 2500 K and CO_2, H_2O, and N_2 as components. In order to generate a structural hot spot as in the experiment, a temperature of 1000 K was imposed at the top boundary. The initial configuration of the computation is illustrated in Fig. 3. The hot wall enabled the creation of a temperature gradient and the triggering of the end-gas auto-ignition. In their study, Peters et al. [8] investigated the temperature history of 13 hot spots with initial temperatures spanning over a range of 120 K. In addition, Mansfield and Wooldridge [23] reported an expected 5 K/mm gradient for typical RCM facilities. Consequently, the temperature gradient used in the present study, approximately 3.5 K/mm, appears realistic. As for the resolution, a mesh distribution at the moment of detonation onset is depicted in Fig. 4.

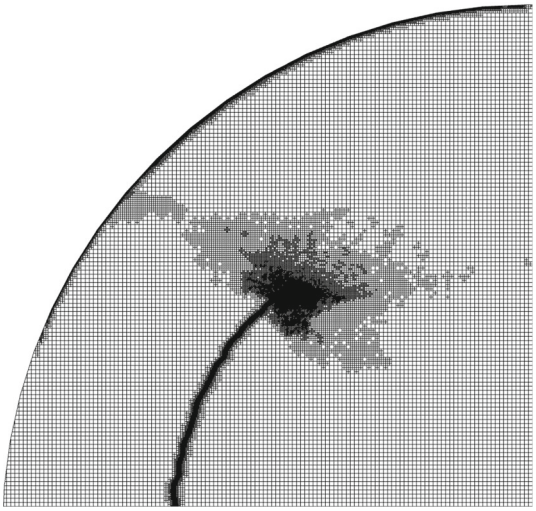

Fig. 4 Mesh distribution at the moment of detonation onset

The governing equations employed in the simulation are the reactive compressible Navier–Stokes equations in which the acceleration due to the gravity has been neglected:

$$\partial_t(\rho) + \nabla \cdot p(\rho \mathbf{u}) = 0, \tag{1}$$

$$\partial_t(\rho \mathbf{u}) + \nabla \cdot p(\rho \mathbf{u}\mathbf{u}) = -\nabla P + \nabla \cdot p\sigma, \tag{2}$$

where

$$\sigma = \mu\left[\nabla \mathbf{u} + (\nabla \mathbf{u})^T\right] - \frac{2}{3}\mu(\nabla \mathbf{u})\mathbf{I}, \tag{3}$$

$$\partial_t(\rho e) + \nabla \cdot p(\rho \mathbf{u} e) = -\nabla \cdot pJ_q + \sigma \nabla \mathbf{u} + \dot{q}, \tag{4}$$

with

$$J_q = -\rho D \nabla h - K \nabla T, \tag{5}$$

$$\partial_t(\rho Y_m) + \nabla \cdot p(\rho \mathbf{u} Y_m) = -\nabla \cdot pJ_m + S_m, \tag{6}$$

with

$$J_m = -\rho D \nabla Y_m. \tag{7}$$

In the above equations, $\mathbf{u}$ is the velocity vector, ρ, P, T are the gas density, pressure, and temperature. Y_m is the mass fraction of species m and S_m is the source term for species m. J_m is the species diffusion flux and J_q is the heat flux. $\dot{q}$ is the energy release rate from chemical reactions, h is the mixture enthalpy, and e is the internal energy. σ is the deviatoric stress tensor, μ is the viscosity, given by a renormalization group, RNG, k-ϵ turbulence model, and I is the identity matrix. D is the mass diffusion coefficient in Fick's law, and K is the thermal conductivity.

A Redlich–Kwong cubic equation is used for the gas state to improve the accuracy under the high temperature and pressure conditions:

$$P = \frac{RT}{v - b} - \frac{a}{v^2 + ubv + wb^2} \tag{8}$$

where a, b, u, and w are constants. v is the volume and R is the universal gas constant.

These conservation equations are integrated in two dimensions. The spatial discretization of the solution domain is performed using the central finite difference method. Specifically, the convection and diffusion terms were discretized as second order. The pressure–velocity coupling in CONVERGE is achieved using a modified pressure implicit with splitting of operators (PISO) algorithm. On the other hand, the time derivative is explicit–implicit discretized with a second-order accuracy,

$$\frac{\phi^{n+1} - \phi^n}{t^{n+1} - t^n} + \frac{1}{2} \cdot \frac{\partial u^n \phi^n}{\partial x} + \frac{1}{2} \cdot \frac{\partial u^{n+1} \phi^{n+1}}{\partial x} = 0 \tag{9}$$

where ϕ is any variable and x is a spatial position.

3 Experimental and numerical results

The present mode of detonation initiation through interaction of the shock wave with the flame was observed during twenty experiments with a good reproducibility, presented in Fig. 2 in the supplementary material. Figure 5 compares the experimental self-luminescence images and the numerical simulations of the SWFID process. The numerical images present the pressure and temperature distribution along with the HCO radical field, which represents the flame front or preheat zone, and the OH radical field which represents the reaction zone. The numerical results reproduce the main features observed experimentally and demonstrate overall qualitative agreement. The initial shock wave propagates downward from the auto-ignition at the top and then interacts with the spherically expanding flame generated by the spark plug. A local thermal explosion with intense luminosity can be observed from 370 to 374 μs at the flame front. At $t = 377$ μs, a curved reaction front near the wall can also be observed on both sides of the experimental image. The occurrence of traverse waves and the near-wall reflection event has been illustrated in the SWRID process [16]. Extracting the propagation path of the near-wall detonation wave from experimental results, the average speed is calculated as 1730 m/s ($M = 3.2$), which means a 6.3% deficit compared to the local Chapman–Jouguet velocity for the mixture ($D_{CJ} = 1847$ m/s). In addition, the velocity of the combustion wave originating from the detonation kernel is calculated to be 1820 m/s, which is roughly coincident with the Chapman–Jouguet velocity.

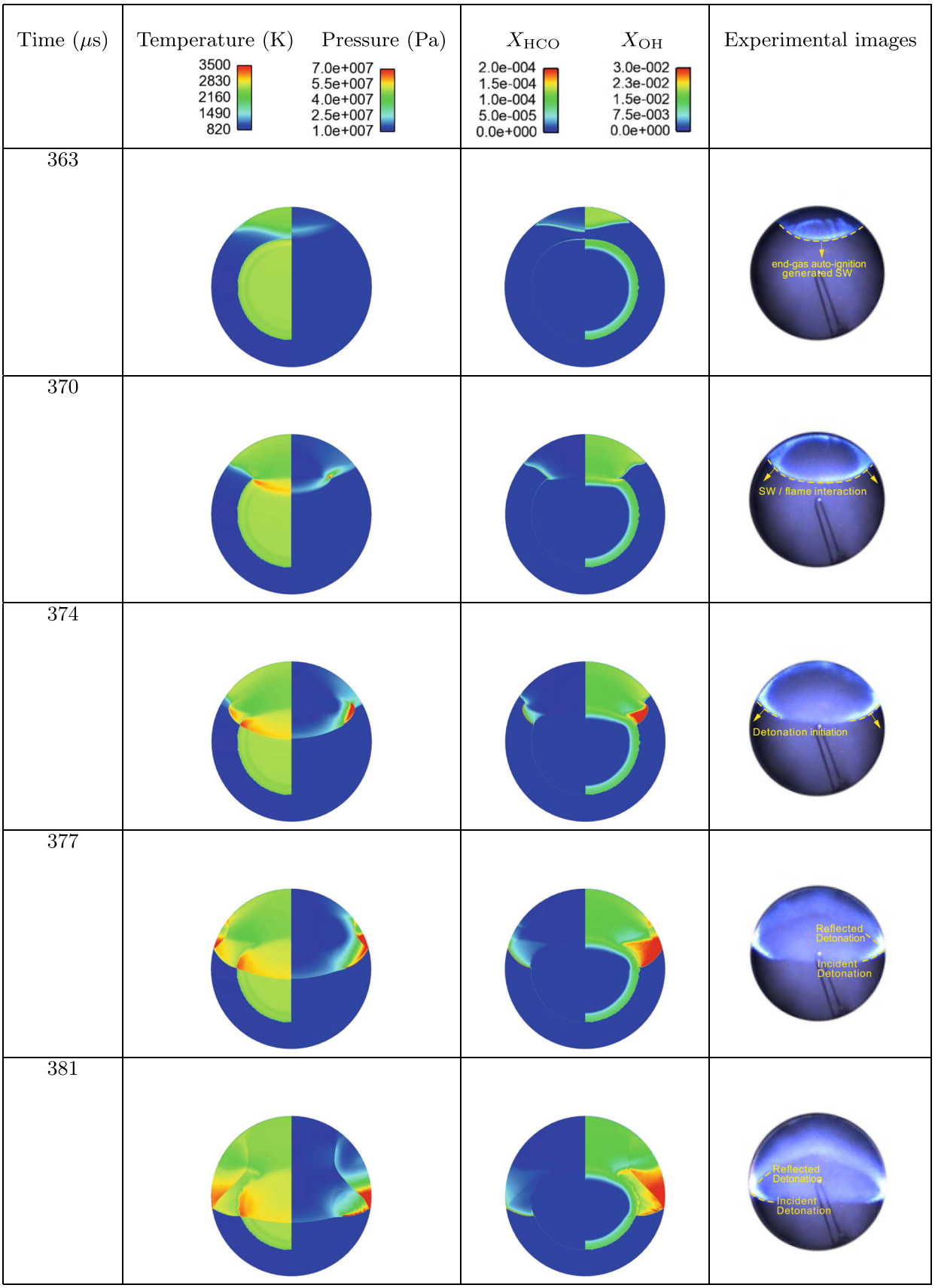

Fig. 5 Numerical and experimental SWFID phenomenon

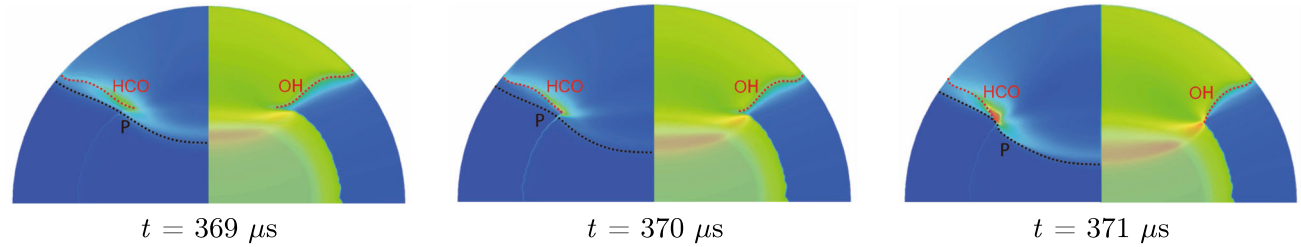

Fig. 6 Superimposed pressure field and HCO front (left half) and temperature field and OH front (right half) at detonation onset. On the left, the front of the shock wave induced by the top wall explosion is also shown as black dashed lines

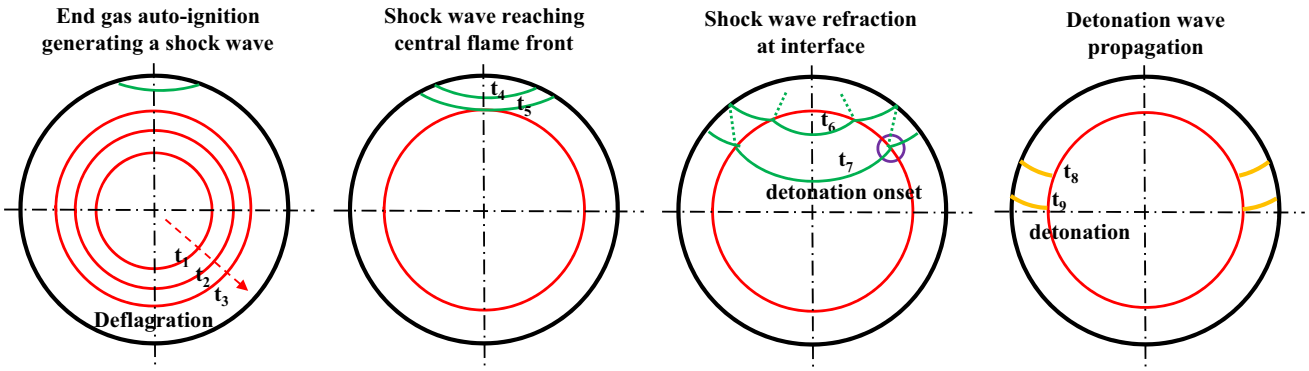

Fig. 7 Main steps of the SWFID process

To gain further insight into the mechanism of detonation initiation, superimposed temperature, pressure, and species concentration fields at detonation onset were displayed in Fig. 6. At $t = 369\,\mu s$, a region of higher pressure and temperature is created at the intersection of the shock fronts propagating in the burnt and in the unburnt gas regions. The pressure at this location is the highest in the computational domain, whereas the maximum temperature is located in the region of burnt gas compressed by the incident shock wave. Nevertheless, the temperature at the interception of the two shock fronts is several hundred kelvin above that of the fresh mixture compressed by the end-gas shock wave. The localized higher temperature enables the flame front to accelerate, $t = 370\,\mu s$, and catches up with the shock front, $t = 371\,\mu s$, to eventually form a self-sustained detonation wave.

4 Discussion

The specific configuration under which super-knock initiation was observed in the present study shows similarities with a well-known gas dynamic problem, shock wave refraction. Such a phenomenon has received considerable attention over the years [24–27]. But due to its high complexity, most studies have focused on straight interfaces separating two non-reactive media [28]. A shock refraction complex is composed of an incident shock (propagating in the primary medium), a transmitted shock (propagating in the secondary medium), and a reflected wave (shock or expansion wave). Depending on different parameters such as the Mach number of the incident shock, the angle of incidence, and the properties of the gases on either side of the interface, a number of regular and irregular shock refractions can be observed as summarized by Han and Yin [29]. Under certain conditions, a free-precursor shock running ahead of the incident shock may be formed [25]. Because of its low density and high temperature, the expanding spherical flame corresponds to a slow–fast interface [26] and acts as a divergent acoustic lens [28]. As noted by Haas and Sturtevant [28], the interaction of a shock wave with cylindrical and spherical interfaces covers the complete range of incidence angles and consequently results in a large variety of refraction configurations. On the basis of the fundamental aspects of shock wave refraction, the SWFID observed in the RCM could be interpreted as follows: (1) the curved shock front originating from the end-gas auto-ignition meets the spherically expanding flame, (2) the refracted shock propagates faster within the burnt gas, which leads to the formation of a regular shock refraction, (3) the region of high temperature and pressure is formed at the interface in the vicinity of the triple point, (4) as the shock propagates along the interface, the angle of incidence increases which leads to a transition from regular to irregular refraction, (5) the free-precursor shock formed is accelerated by propagating in a preconditioned region, (6) detonation onset takes place behind the free-precursor shock. A simpli-

fied schematic of this mode of super-knock initiation through the SWFID process is shown in Fig. 7.

It should be emphasized that the details of the shock–flame interaction could not be well captured by the present simulations due to insufficient numerical resolution and the lack of shock capturing algorithm. The perturbations on the central flame front can also be attributed to the mesh resolution. Future work will focus on better resolving this interaction, but one must keep in mind that the smallest chemical length scales are extremely small, e.g., on the order of 0.1 nm (based on ZND calculation) under super-knock conditions. Despite the limitations of the experimental visualizations and simulations, the present results are valuable in demonstrating the possibility of detonation initiation through a shock wave refraction process. To the best of the authors' knowledge, this is the first time that evidence of such a phenomenon is revealed. This is probably due to the extreme thermodynamic states encountered under super-knock relevant conditions. Most detonation studies, especially with visualization, are limited to sub-atmospheric or atmospheric initial pressures [30,31]. Similar conclusions can be drawn for shock wave–flame interaction studies. Likely due to the fact that the sensitivity to detonation of typical combustible mixtures is too weak at low initial pressure, detonation initiation at the interface was not observed and the studies have focused on the dynamics of the distortion of the burnt gas volume induced by the shock wave or on the ignition/detonation onset following shock reflection [32–39].

The present experimental and numerical results, along with our previous study on SWRID [16], indicate that the classical super-knock theory, i.e., the acoustic coupling theory from Bradley, along with the associated one-dimensional simulations with a temperature gradient, should be interpreted with great care in the context of super-knock initiation. Bradley's theory stipulates that detonation onset is achieved through resonant acoustic coupling. Following this idea and further considering the turbulent fluctuations of the flow field, Peters et al. [8] obtained the statistics of detonation probability in an ICE. Peters' study showed that the detonation probability is maximum in the central area of the combustion chamber where turbulent fluctuations are minimum. In contrary to Peters' results, the RCM experiments [4,16] demonstrate that the super-knock is usually initiated close to the wall after the end-gas shock wave has interacted with the confinement, the flame, or another shock wave. This interaction modifies significantly the local thermodynamic state and consequently the conditions for which detonation onset can take place. Therefore, when the one-dimensional acoustic coupling theory is utilized to interpret the detonation initiation for a case in which the shock wave is interacting with other factors, the thermodynamic state and shock characteristics after the interaction has taken place should be considered. This observation is consistent with the study of Roberts et al. [40]. By performing 3-D numerical simulations of super-knock in a spark ignition engine, they noted that detonation onset does not always originate from the first auto-ignition spot. This implies that the conditions at the end of compression may or may not be the relevant ones to utilize Bradley's DDT diagram.

5 Conclusion

In the present study, one mode of super-knock initiation, referred to as shock wave and flame front induced detonation, has been investigated. A combination of experimental and numerical approaches was used to analyze the detonation initiation process of stoichiometric iso-octane/air mixtures in an RCM under engine-relevant conditions. The interaction between the shock wave generated by end-gas auto-ignition and the spherical expanding flame creates a region of high pressure and high temperature which enables the acceleration of the flame front and, eventually, the detonation onset. While similarities could be seen with the shock wave refraction phenomenon, additional work is needed to clearly quantify the conditions under which super-knock occurs. Highly resolved experimental and numerical methods are required for further investigation. In particular, the velocity of the induction shock wave and its angle of incidence with the expanding flame are of fundamental importance to characterize the configuration of the shock wave refraction.

Acknowledgements This work was performed at Tsinghua University and was supported by the National Natural Science Foundation of China (Grant Nos. 91541206, 51706121), Tsinghua University Initiative Scientific Research Program (Grant No. 20161080114) and China Postdoctoral Science Foundation (Grant No. 2017T100076). Remy Mével was supported by a start-up fund of the Center for Combustion Energy of Tsinghua University. The authors are grateful to J.E. Shepherd from Caltech for useful discussions.

References

1. Shafiee, S., Topal, E.: When will fossil fuel reserves be diminished? Energy Policy **37**, 181–189 (2009). https://doi.org/10.1016/j.enpol.2008.08.016
2. Smith, K., Frumkin, H., Balakrishnan, K., Butler, C., Chafe, Z., Fairlie, I., Kinney, P., Kjellstrom, T., Mauzerall, D., McKone, T., McMichael, A., Schneider, M.: Energy and human health. Annu. Rev. Public Health **34**(1), 159–188 (2013). https://doi.org/10.1146/annurev-publhealth-031912-114404
3. Seinfeld, J., Pandis, S.: Atmospheric Chemistry and Physics: From Air Pollution to Climate Change. Wiley, Toronto (1998)
4. Wang, Z., Qi, Y., He, X., Wang, J., Shuai, S., Law, C.K.: Analysis of pre-ignition to super-knock: hotspot-induced deflagration to detonation. Fuel **144**, 222–227 (2015). https://doi.org/10.1016/j.fuel.2014.12.061
5. Qi, Y., Wang, Z., Wang, J., He, X.: Effects of thermodynamic conditions on the end gas combustion mode associated with engine

knock. Combust. Flame **162**, 4119–4128 (2015). https://doi.org/10.1016/j.combustflame.2015.08.016
6. Wang, Z., Liu, H., Reitz, R.: Knocking combustion in spark-ignition engines. Prog. Energy Combust. Sci. **61**, 78–112 (2017). https://doi.org/10.1016/j.pecs.2017.03.004
7. Grogan, K.P., Goldsborough, S.S., Ihme, M.: Ignition regimes in rapid compression machines. Combust. Flame **162**, 3071–3080 (2015). https://doi.org/10.1016/j.combustflame.2015.03.020
8. Peters, N., Kerschgens, B., Paczko, G.: Super-knock prediction using a refined theory of turbulence. SAE Int. J. Engines **6**(2), 953–967 (2013). https://doi.org/10.4271/2013-01-1109
9. Im, H.G., Pal, P., Wooldridge, M.S., Mansfield, A.B.: A regime diagram for autoignition of homogeneous reactant mixtures with turbulent velocity and temperature fluctuations. Combust. Sci. Technol. **187**, 1263–1275 (2015). https://doi.org/10.1080/00102202.2015.1034355
10. Sankaran, R., Im, H.G., Hawkes, E.R., Chen, J.H.: The effects of non-uniform temperature distribution on the ignition of a lean homogeneous hydrogen–air mixture. Proc. Combust. Inst. **30**, 875–882 (2005). https://doi.org/10.1016/j.proci.2004.08.176
11. Zeldovich, Y.B.: Regime classification of an exothermic reaction with nonuniform initial conditions. Combust. Flame **39**, 211–214 (1980). https://doi.org/10.1016/0010-2180(80)90017-6
12. Bradley, D., Morley, C., Gu, X.J., Emerson, D.R.: Amplified pressure waves during autoignition: relevance to CAI engines. SAE Technical Paper 2002-01-2868 (2002). https://doi.org/10.4271/2002-01-2868
13. Gu, X.J., Emerson, D.R., Bradley, D.: Modes of reaction front propagation from hot spots. Combust. Flame **133**, 63–74 (2003). https://doi.org/10.1016/S0010-2180(02)00541-2
14. Dai, P., Chen, Z.: Supersonic reaction front propagation initiated by a hot spot in *n*-heptane/air mixture with multistage ignition. Combust. Flame **162**, 4183–4193 (2015). https://doi.org/10.1016/j.combustflame.2015.08.002
15. Dai, P., Chen, Z., Chen, S., Ju, Y.: Numerical experiments on reaction front propagation in *n*-heptane/air mixture with temperature gradient. Proc. Combust. Inst. **35**, 3045–3052 (2015). https://doi.org/10.1016/j.proci.2014.06.102
16. Wang, Z., Qi, Y., Liu, H., Zhang, P., He, X., Wang, J.: Shock wave reflection induced detonation (SWRID) under high pressure and temperature condition in closed cylinder. Shock Waves **26**, 687–691 (2016). https://doi.org/10.1007/s00193-016-0677-5
17. Di, H., He, X., Zhang, P., Wang, Z., Wooldridge, M.S., Law, C.K., Wang, C., Shuai, S., Wang, J.: Effects of buffer gas composition on low temperature ignition of iso-octane and n-heptane. Combust. Flame **161**, 2531–2538 (2014). https://doi.org/10.1016/j.combustflame.2014.04.014
18. Wang, Z., Li, F., Wang, Y.: A generalized kinetic model with variable octane number for engine knock prediction. Fuel **188**, 489–499 (2017). https://doi.org/10.1016/j.fuel.2016.10.067
19. Tanaka, S., Ayala, F., Keck, J.C.: A reduced chemical kinetic model for HCCI combustion of primary reference fuels in a rapid compression machine. Combust. Flame **133**, 467–481 (2003). https://doi.org/10.1016/S0010-2180(03)00057-9
20. Tsurushima, T.: A new skeletal PRF kinetic model for HCCI combustion. Proc. Combust. Inst. **32**(2), 2835–2841 (2009). https://doi.org/10.1016/j.proci.2008.06.018
21. Fieweger, K., Blumenthal, R., Adomeit, G.: Self-ignition of S.I. engine model fuels: a shock tube investigation at high pressure. Combust. Flame **109**, 599–619 (1997). https://doi.org/10.1016/S0010-2180(97)00049-7
22. Richards, K.J., Senecal, P.K., Pomraning, E.: CONVERGE (v2.2). Convergent Science, Inc., Madison (2015)
23. Mansfield, A.B., Wooldridge, M.S.: High-pressure low-temperature ignition behavior of syngas mixtures. Combust. Flame **161**(9), 2242–2251 (2014). https://doi.org/10.1016/j.combustflame.2014.03.001
24. Henderson, L.F.: The refraction of a plane shock wave at a gas interface. J. Fluid Mech. **26**, 607–637 (1966). https://doi.org/10.1017/S0022112066001435
25. Abd-El-Fattah, A.M., Henderson, L.F., Lozzi, A.: Precursor shock waves at a slow–fast gas interface. J. Fluid Mech. **76**, 157–176 (1976). https://doi.org/10.1017/S0022112076003182
26. Abd-El-Fattah, A.M., Henderson, L.F.: Shock waves at a slow–fast gas interface. J. Fluid Mech. **89**, 79–95 (1978). https://doi.org/10.1017/S0022112078002475
27. Henderson, L.F.: On the refraction of shock waves. J. Fluid Mech. **198**, 365–386 (1989). https://doi.org/10.1017/S0022112089000170
28. Haas, J.F., Sturtevant, B.: Interaction of weak shock waves with cylindrical and spherical gas inhomogeneities. J. Fluid Mech. **181**, 41–76 (1987). https://doi.org/10.1017/S0022112087002003
29. Han, Z., Yin, X.: Shock Dynamics. Springer, Dordrecht (1993). https://doi.org/10.1007/978-94-017-2995-6
30. Austin, J.M., Pintgen, F., Shepherd, J.E.: Reaction zones in highly unstable detonations. Proc. Combust. Inst. **30**, 1849–1857 (2005). https://doi.org/10.1016/j.proci.2004.08.157
31. Radulescu, M.I., Sharpe, G.J., Law, C.K., Lee, J.H.S.: The hydrodynamic structure of unstable cellular detonations. J. Fluid Mech. **580**, 31–78 (2007). https://doi.org/10.1017/S0022112007005046
32. Ju, Y., Shimano, A., Inoue, O.: Vorticity generation and flame distortion induced by shock flame interaction. Proc. Combust. Inst. **27**(1), 735–74 (1998). https://doi.org/10.1016/S0082-0784(98)80467-0
33. Picone, J.M., Oran, E.S., Boris, J.P., Young, T.R.: Theory of vorticity generation by shock wave and flame interactions. In: Dynamics of Shock Waves, Explosions, and Detonations, Progress in Astronautics and Aeronautics, vol. 94, AIAA (1985). https://doi.org/10.2514/5.9781600865695.0429.0448
34. Markstein, G.H.: A shock tube study of flame front-pressure wave interactions. Proc. Combust. Inst. **6**, 387–398 (1957). https://doi.org/10.1016/S0082-0784(57)80054-X
35. Thomas, G.O., Bambrey, R., Brown, C.: Experimental observations of flame acceleration and transition to detonation following shock–flame interaction. Combust. Theory Model. **5**, 573–594 (2001). https://doi.org/10.1088/1364-7830/5/4/304
36. Dong, G., Fan, B., Ye, J.: Numerical investigation of ethylene flame bubble instability induced by shock waves. Shock Waves **17**, 409–419 (2008). https://doi.org/10.1007/s00193-008-0124-3
37. Dong, G., Fan, B., Gui, M., Li, B.: Numerical simulations of interactions between a flame bubble with an incident shock wave and its focusing wave. J. Mech. Eng. Sci. **223**(10), 2357–2367 (2009). https://doi.org/10.1243/09544062JMES1467
38. Chen, X., Dong, G., Jiang, H.: A three-dimensional numerical study on instability of sinusoidal flame induced by multiple shock waves. Acta Mech. Sin. **33**(2), 316–326 (2017). https://doi.org/10.1007/s10409-017-0639-x
39. Ivanov, M.F., Kiverin, A.D.: Generation of high pressures during the shock wave–flame interaction. High Temp. **53**(5), 668–676 (2015). https://doi.org/10.1134/S0018151X15030086
40. Robert, A., Richard, S., Colin, O., Poinsot, T.: LES study of deflagration to detonation mechanisms in a downsized spark ignition engine. Combust. Flame **162**(7), 2788–2807 (2015). https://doi.org/10.1016/j.combustflame.2015.04.010